LA-UR-95-2876

Title: Surface Strains Due to Face Loading of a Slot in a Layered Half-Space

Author(s): M.B.Prime & I. Finnie

Submitted to: ASME Journal of Engineering Materials and Technology

Prime, M. B., and Finnie, I., 1996, "Surface strains due to face loading of a slot in a layered half-space," Journal of Engineering Materials and Technology, 118(3), pp. 410-418.

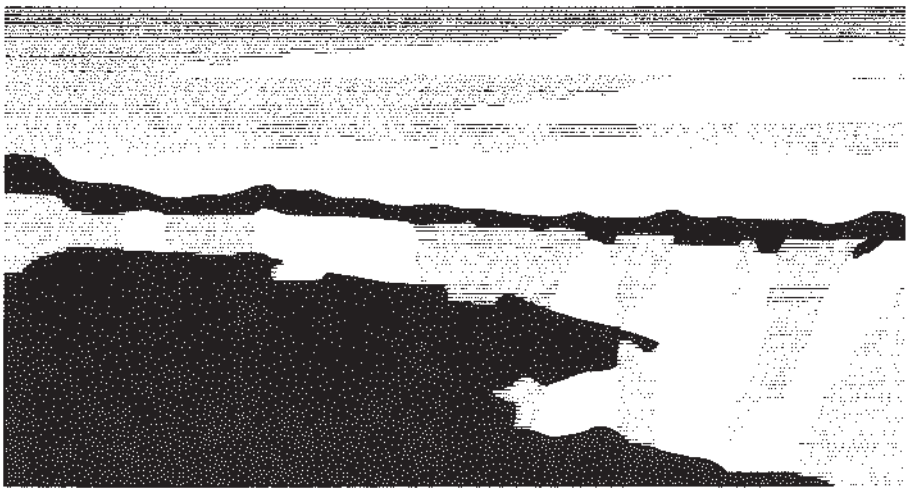

Los Alamos
NATIONAL LABORATORY

Form No. 836 R5
ST 2629 10/91

JEMT #96-22, Revised

Surface Strains Due to Face Loading of a Slot in a Layered Half-Space

M. B. Prime
Technical Staff Member, Associate Member ASME

Los Alamos National Laboratory
Los Alamos, NM 87545

I. Finnie
Professor Emeritus, Honorary Member ASME

Department of Mechanical Engineering
University of California
Berkeley, CA 94720

Abstract

A solution is presented that will allow the compliance method for residual stress measurement to be applied to layered materials. The solution is for surface strains due to arbitrary normal stress loading on the faces of a slot in a layered half-space. The materials are homogeneous isotropic elastic with different elastic constants and the slot may penetrate into the substrate. The solution is accomplished using the body force method and the solution for a point force in two bonded half spaces. The results indicate that, for residual stress measurement, the effects of the substrate properties are significant for materials with elastic moduli differing by 50 percent or more when the slot penetrates to at least one-half of the layer thickness.

Introduction

It is difficult to measure the variation of residual stress with depth, especially in a layer of one material on a substrate of another where the elastic constants differ. Knowledge of these stresses is very useful since, for example, they can cause cracking or debonding of a cladded layer. All current residual stress measurement techniques suffer from limitations. And in the rare instances when they have been applied to layered materials, they generally ignore the effect of a substrate with different elastic constants. The use of the compliance method (Cheng et al., 1994) to address some of these limitations motivated this work. A more detailed discussion of the various techniques is saved for another paper where the result here is applied experimentally to residual stress measurement.

The compliance method has been successfully applied to measurement of residual stresses for single materials. A slot is introduced incrementally into a body containing residual stress. The resulting strain at a location on the surface is measured and used to calculate the stress variation with depth. To apply the method it is necessary to calculate the compliance functions, or surface strains for arbitrary face loading of a slot, for the relevant geometry. Cheng and Finnie (1993) performed the calculation for a surface slot in a single material using the body force method (Nisitani 1978).

In this work the compliance functions are calculated for a surface slot in a layered half-space consisting of two homogeneous isotropic elastic materials. The calculation technique is a new extension of the body force method. In the body force method, the stress solutions for a point force in an unnotched body are used to solve the problem of stresses in a body containing a notch. Body forces, or continuously embedded point forces, are applied to the boundary of the prospective notch. Their magnitude is adjusted to satisfy the boundary conditions. Here, because the point force solution for the exact geometry is not available, the body forces are applied to the site of a prospective free surface as well as the notch. Noda et al. (1992) used a similar approach, but to solve for the stress field near the notch. Here the

stresses at the free surface are required, which adds the complexity of solving for stresses remote from the notch and at a location where body forces are applied.

The body forced method is chosen over other methods such as the finite element method or the boundary integral method for several reasons. The calculations must be performed for a large number of permutations of slot depth, face loading, and layer thickness. Meshing only the boundaries, as compared to using finite elements, is simpler, quicker, can be more easily automated, and allows more local refinement for the same computation time. The body force method is stress based and the quantity of interest is strain, which is given directly from the stress components. Displacement based methods, including finite elements and boundary integral, require differentiation to get strain, which decreases accuracy in a numerical solution. The body force method handles stress singularities, such as at the tip of a crack, with no special attention or special elements. And the body force method is conceptually simpler to understand and implement than the boundary integral method.

Analysis

Fig. 1 shows the problem to be solved. A slot of depth d and width $2w$ in a layered half-space is loaded with an arbitrary normal stress distribution, symmetrical with respect to the y-axis, on its faces. The surface layer has different elastic properties then the substrate and thickness h. This loading corresponds to the residual stresses released by making the slot. The response at a strain gage on the surface is desired. To apply the body force method a point force solution for the unnotched body is required. Unfortunately, the solution for a point force in a layered half-space is not available. The closest available solution is for a point force in two bonded half-spaces, as shown in Fig. 2. It was first obtained by Frasier and Rongved (1957) and also given later as a subcase of more complex solutions (Dundurs and Hetényi, 1961, 1962, and Wu and Chou, 1982). The solutions were all carefully checked for accuracy, and that given by Dundurs and Hetényi was found to be the only one error free. The stress

components in the coordinate system used here are given in the Appendix. The errors found in the other solutions and details on converting between solutions are given in Prime (1994).

The following notation is used in referring to stresses due to a point force: $\sigma_{xi}^{Pj}(x,y,s,t)$ is the x component of normal stress at (x,y) in material i (i=1,2) due to horizontal (x-direction) force P at (s,t) in material j (j=1,2). Q instead of P refers to a vertical (y-direction) force and τ_{xy} is shear stress.

Beginning with two bonded half-spaces, continuously embedded point forces $f_x(s,t)$ and $f_y(s,t)$ are applied to the desired sites of the slot bottom ($y=h-d$, $-w<x<w$), slot sides ($x=\pm w$, $h-d<y<h$) and free surface ($y=h$, $x>w$ and $x<-w$), see Fig. 3. The magnitudes of the applied forces must be adjusted so that the stresses on the contours match those of Fig. 1. By applying additional point forces, symmetric with respect to $y=h$, to the mirror image of the slot bottom ($y=h+d$, $-w<x<w$) and slot sides ($x=\pm w$, $h<y<h+d$), the shear stress on the free surface is made small in advance. This will accelerate convergence of the numerical solution. The symmetry as illustrated in Fig. 3 applies only to the case of normal loading on the slot face. Anti-symmetric forces would be used to consider shear loading.

Note that following equation is written **without** considering the signs of the point forces implied by the symmetry in Fig. 3. The equation is, therefore, applicable to general loading. When the equation is discretized the signs are included explicitly.

The normal stress on the bottom of the slot can be expressed as a sum of the contributions from all portions of the contour.

$$
\begin{aligned}
\sigma_y(x,h-d) = & \int_{-w}^{w}\left[f_x(s,h-d)\sigma_{y**}^{P*}(x,h-d,s,h-d)+f_y(s,h-d)\sigma_{y**}^{Q*}(x,h-d,s,h-d)\right]ds \\
& + \int_{-w}^{w}\left[f_x(s,h+d)\sigma_{y**}^{P1}(x,h-d,s,h+d)+f_y(s,h+d)\sigma_{y**}^{Q1}(x,h-d,s,h+d)\right]ds \\
& + \int_{h-d}^{h+d}\left[f_x(w,t)\sigma_{y**}^{P*}(x,h-d,w,t)+f_y(w,t)\sigma_{y**}^{Q*}(x,h-d,w,t)\right]dt \\
& + \int_{h-d}^{h+d}\left[f_x(-w,t)\sigma_{y**}^{P*}(x,h-d,-w,t)+f_y(-w,t)\sigma_{y**}^{Q*}(x,h-d,-w,t)\right]dt \\
& + \left\{\int_{-\infty}^{-w}+\int_{w}^{\infty}\right\}\left[f_x(s,h)\sigma_{y**}^{P1}(x,h-d,s,h)+f_y(s,h)\sigma_{y**}^{Q1}(x,h-d,s,h)\right]ds
\end{aligned}
\tag{1}
$$

where * = 1 for t of (x,y,s,t) positive and 2 for t negative, and ** = 1 for y positive and 2 for y negative.

To conserve space the equations for the shear stress on the slot bottom, $\tau_{xy}(x,h-d)$, the stresses on the slot sides, $\sigma_x(\pm w,y)$ and $\tau_{xy}(\pm w,y)$, and the stresses on the free surface, $\sigma_y(x,h)$ and $\tau_{xy}(x,h)$, are omitted now but included in their discretized form later. They are of similar form to Eq. (1).

The unknown body forces $f_x(s,t)$ and $f_y(s,t)$ must be determined numerically. The inherent symmetry in the problem, as illustrated in Fig. 3, is used to minimize calculation. Making use of this symmetry, the contour is discretized. Half of the slot bottom is divided into n_1 intervals from $x = 0$ to $x = w$. One of the slot sides is divided into n_2 intervals from $y = h\text{-}d$ to $y = h$. And half of the free surface is divided into n_3 intervals from $x = w$ to $x = s_{max}$ (the value of s_{max} is discussed later). The stresses on each of these contours is calculated as a sum of the contributions from point forces on all of the contours. Consider the body forces within each interval as constant with magnitudes f_{xi} and f_{yi} for the i^{th} interval. This gives $2N$ equations in $2N$ unknowns where N is $n_1+n_2+n_3$:

$$\begin{bmatrix} & \\ & \\ & \\ & \\ & \\ & \\ & \\ & \\ & \\ & \end{bmatrix} \begin{Bmatrix} f_{x1} \\ f_{y1} \\ \cdots \\ f_{xi} \\ f_{yi} \\ \cdots \\ f_{xN} \\ f_{yN} \end{Bmatrix} = \begin{Bmatrix} \sigma_1 \\ \tau_1 \\ \cdots \\ \sigma_i \\ \tau_i \\ \cdots \\ \sigma_N \\ \tau_N \end{Bmatrix} \tag{2}$$

The entries in the above matrix are calculated from the following equations, which are the discretized form of Eq. (1) and its counterparts. The normal stresses on the slot bottom are now given by

$$\begin{aligned} \sigma_y(x,h-d) = \sum_{i=1}^{n_1} & \left\{ \begin{array}{l} \int_{s_i}^{s_{i+1}} \left[f_{xi}\sigma_{y**}^{P*}(x,h-d,s,h-d) + f_{yi}\sigma_{y**}^{Q*}(x,h-d,s,h-d) \right] ds + \\ \int_{s_{i+1}}^{s_i} \left[f_{xi}\sigma_{y**}^{P*}(x,h-d,-s,h-d) - f_{yi}\sigma_{y**}^{Q*}(x,h-d,-s,h-d) \right] ds + \\ \int_{s_i}^{s_{i+1}} \left[f_{xi}\sigma_{y**}^{P1}(x,h-d,s,h+d) - f_{yi}\sigma_{y**}^{Q1}(x,h-d,s,h+d) \right] ds + \\ \int_{s_{i+1}}^{s_i} \left[f_{xi}\sigma_{y**}^{P1}(x,h-d,-s,h+d) + f_{yi}\sigma_{y**}^{Q1}(x,h-d,-s,h+d) \right] ds \end{array} \right\} \\ + \sum_{i=n_1+1}^{n_1+n_2} & \left\{ \begin{array}{l} \int_{t_i}^{t_{i+1}} \left[f_{xi}\sigma_{y**}^{P*}(x,h-d,w,t) + f_{yi}\sigma_{y**}^{Q*}(x,h-d,w,t) \right] dt + \\ \int_{t_{i+1}}^{t_i} \left[-f_{xi}\sigma_{y**}^{P*}(x,h-d,-w,t) + f_{yi}\sigma_{y**}^{Q*}(x,h-d,-w,t) \right] dt + \\ \int_{t_{i+1}}^{t_i} \left[-f_{xi}\sigma_{y**}^{P1}(x,h-d,w,2h-t) + f_{yi}\sigma_{y**}^{Q1}(x,h-d,w,2h-t) \right] dt + \\ \int_{t_i}^{t_{i+1}} \left[f_{xi}\sigma_{y**}^{P1}(x,h-d,-w,2h-t) + f_{yi}\sigma_{y**}^{Q1}(x,h-d,-w,2h-t) \right] dt \end{array} \right\} \\ + \sum_{i=n_1+n_2+1}^{n_1+n_2+n_3} & \left\{ \begin{array}{l} \int_{s_i}^{s_{i+1}} \left[f_{xi}\sigma_{y**}^{P1}(x,h-d,s,h) + f_{yi}\sigma_{y**}^{Q1}(x,h-d,s,h) \right] ds + \\ \int_{s_{i+1}}^{s_i} \left[f_{xi}\sigma_{y**}^{P1}(x,h-d,-s,h) - f_{yi}\sigma_{y**}^{Q1}(x,h-d,-s,h) \right] ds \end{array} \right\} \end{aligned} \tag{3}$$

The normal stresses on the slot side are

$$\sigma_x(w,y)=\sum_{i=1}^{n_1}\left\{\begin{array}{l}\int_{si}^{si+1}\left[f_{xi}\sigma_{x**}^{P*}(w,y,s,h-d)+f_{yi}\sigma_{x**}^{Q*}(w,y,s,h-d)\right]ds+\\ \int_{si+1}^{si}\left[f_{xi}\sigma_{x**}^{P*}(w,y,-s,h-d)-f_{yi}\sigma_{x**}^{Q*}(w,y,-s,h-d)\right]ds+\\ \int_{si}^{si+1}\left[f_{xi}\sigma_{x**}^{P1}(w,y,s,h+d)-f_{yi}\sigma_{x**}^{Q1}(w,y,s,h+d)\right]ds+\\ \int_{si}^{si+1}\left[f_{xi}\sigma_{x**}^{P1}(w,y,-s,h+d)+f_{yi}\sigma_{x**}^{Q1}(w,y,-s,h+d)\right]ds\end{array}\right\}$$

$$+\sum_{i=n_1+1}^{n_1+n_2}\left\{\begin{array}{l}\int_{ti}^{ti+1}\left[f_{xi}\sigma_{x**}^{P*}(w,y,w,t)+f_{yi}\sigma_{x**}^{Q*}(w,y,w,t)\right]dt+\\ \int_{ti+1}^{ti}\left[-f_{xi}\sigma_{x**}^{P*}(w,y,-w,t)+f_{yi}\sigma_{x**}^{Q*}(w,y,-w,t)\right]dt+\\ \int_{ti}^{ti+1}\left[-f_{xi}\sigma_{x**}^{P1}(w,y,w,2h-t)+f_{yi}\sigma_{x**}^{Q1}(w,y,w,2h-t)\right]dt+\\ \int_{ti}^{ti+1}\left[f_{xi}\sigma_{x**}^{P1}(w,y,-w,2h-t)+f_{yi}\sigma_{x**}^{Q1}(w,y,-w,2h-t)\right]dt\end{array}\right\} \quad (4)$$

$$+\sum_{i=n_1+n_2+1}^{n_1+n_2+n_3}\left\{\begin{array}{l}\int_{si}^{si+1}\left[f_{xi}\sigma_{x**}^{P1}(w,y,s,h)+f_{yi}\sigma_{x**}^{Q1}(w,y,s,h)\right]ds+\\ \int_{si+1}^{si}\left[f_{xi}\sigma_{x**}^{P1}(w,y,-s,h)-f_{yi}\sigma_{x**}^{Q1}(w,y,-s,h)\right]ds\end{array}\right\}$$

The normal stresses on the free surface are

$$\sigma_y(x,h)=\sum_{i=1}^{n_1}\left\{\begin{array}{l}\int_{s_i}^{s_{i+1}}\left[f_{xi}\sigma_{y1}^{P*}(x,h,s,h-d)+f_{yi}\sigma_{y1}^{Q*}(x,h,s,h-d)\right]ds+\\ \int_{s_i}^{s_{i+1}}\left[f_{xi}\sigma_{y1}^{P*}(x,h,-s,h-d)-f_{yi}\sigma_{y1}^{Q*}(x,h,-s,h-d)\right]ds+\\ \int_{s_i}^{s_{i+1}}\left[f_{xi}\sigma_{y1}^{P1}(x,h,s,h+d)-f_{yi}\sigma_{y1}^{Q1}(x,h,s,h+d)\right]ds+\\ \int_{s_i}^{s_{i+1}}\left[f_{xi}\sigma_{y1}^{P1}(x,h,-s,h+d)+f_{yi}\sigma_{y1}^{Q1}(x,h,-s,h+d)\right]ds\end{array}\right\}$$
$$+\sum_{i=n_1+1}^{n_1+n_2}\left\{\begin{array}{l}\int_{t_i}^{t_{i+1}}\left[f_{xi}\sigma_{y1}^{P*}(x,h,w,t)+f_{yi}\sigma_{y1}^{Q*}(x,h,w,t)\right]dt+\\ \int_{t_i}^{t_{i+1}}\left[-f_{xi}\sigma_{y1}^{P*}(x,h,-w,t)+f_{yi}\sigma_{y1}^{Q*}(x,h,-w,t)\right]dt+\\ \int_{t_i}^{t_{i+1}}\left[-f_{xi}\sigma_{y1}^{P1}(x,h,w,2h-t)+f_{yi}\sigma_{y1}^{Q1}(x,h,w,2h-t)\right]dt+\\ \int_{t_i}^{t_{i+1}}\left[f_{xi}\sigma_{y1}^{P1}(x,h,-w,2h-t)+f_{yi}\sigma_{y1}^{Q1}(x,h,-w,2h-t)\right]dt\end{array}\right\}$$
$$+\sum_{i=n_1+n_2+1}^{n_1+n_2+n_3}\left\{\begin{array}{l}\int_{s_i}^{s_{i+1}}\left[f_{xi}\sigma_{y1}^{P1}(x,h,s,h)+f_{yi}\sigma_{y1}^{Q1}(x,h,s,h)\right]ds+\\ \int_{s_i}^{s_{i+1}}\left[f_{xi}\sigma_{y1}^{P1}(x,h,-s,h)-f_{yi}\sigma_{y1}^{Q1}(x,h,-s,h)\right]ds\end{array}\right\} \quad (5)$$

The signs in Eqs. (3)-(5) are given by considering the signs of the point forces in Fig. 3 and the direction of integration for the various contours. The equations for the shear stresses on these surfaces, are given by substituting τ_{xy} for σ_y throughout Eqs. (3) and (5), and τ_{xy} for σ_x throughout Eq. (4).

Now the values of the stresses on the right-hand sides of Eq. (2) are set equal to the value within each interval given by the desired solution, Fig. 1. These are zero except for the normal stresses on the slot side. Eq. (2) can now be solved directly for the unknown f_{xi} and f_{yi}. The tangential stress on the free surface is then given by

$$\begin{aligned}\sigma_x(x_g,h) = &\sum_{i=1}^{n_1}\left\{\begin{array}{l}\int_{s_i}^{s_{i+1}}\left[f_{xi}\sigma_{x1}^{P*}(x_g,h,s,h-d)+f_{yi}\sigma_{x1}^{Q*}(x_g,h,s,h-d)\right]ds+\\ \int_{s_i}^{s_{i+1}}\left[f_{xi}\sigma_{x1}^{P*}(x_g,h,-s,h-d)-f_{yi}\sigma_{x1}^{Q*}(x_g,h,-s,h-d)\right]ds+\\ \int_{s_i}^{s_{i+1}}\left[f_{xi}\sigma_{x1}^{P*}(x_g,h,s,h+d)-f_{yi}\sigma_{x1}^{Q*}(x_g,h,s,h+d)\right]ds+\\ \int_{s_i}^{s_{i+1}}\left[f_{xi}\sigma_{x1}^{P*}(x_g,h,-s,h+d)+f_{yi}\sigma_{x1}^{Q*}(x_g,h,-s,h+d)\right]ds\end{array}\right\}\\ &+\sum_{i=n_1+1}^{n_1+n_2}\left\{\begin{array}{l}\int_{t_i}^{t_{i+1}}\left[f_{xi}\sigma_{x1}^{P*}(x_g,h,w,t)+f_{yi}\sigma_{x1}^{Q*}(x_g,h,w,t)\right]dt+\\ \int_{t_i}^{t_{i+1}}\left[-f_{xi}\sigma_{x1}^{P*}(x_g,h,-w,t)+f_{yi}\sigma_{x1}^{Q*}(x_g,h,-w,t)\right]dt+\\ \int_{t_i}^{t_{i+1}}\left[-f_{xi}\sigma_{x1}^{P*}(x_g,h,w,2h-t)+f_{yi}\sigma_{x1}^{Q*}(x_g,h,w,2h-t)\right]dt+\\ \int_{t_i}^{t_{i+1}}\left[f_{xi}\sigma_{x1}^{P*}(x_g,h,-w,2h-t)+f_{yi}\sigma_{x1}^{Q*}(x_g,h,-w,2h-t)\right]dt\end{array}\right\}\\ &+\sum_{i=n_1+n_2+1}^{n_1+n_2+n_3}\left\{\begin{array}{l}\int_{s_i}^{s_{i+1}}\left[f_{xi}\sigma_{x1}^{P1}(x_g,h,s,h)+f_{yi}\sigma_{x1}^{Q1}(x_g,h,s,h)\right]ds+\\ \int_{s_i}^{s_{i+1}}\left[f_{xi}\sigma_{x1}^{P1}(x_g,h,-s,h)-f_{yi}\sigma_{x1}^{Q1}(x_g,h,-s,h)\right]ds\end{array}\right\}\end{aligned} \tag{6}$$

From which the strain, i.e., the compliance, is given as

$$\varepsilon_x(x_g,h) = \frac{\sigma_x(x_g,h)}{E_1'} \tag{7}$$

where $E' = E$ for plane stress and $E' = E/(1-\nu^2)$ for plane strain with E the elastic modulus and ν Poisson's ratio. The corresponding plane stress or plane strain point force solution must also be used, which only involves a change in one constant (see Appendix). For residual stress measurement, where the slot width is usually very narrow compared to the thickness of the part, the plane strain solution is generally used.

Numerical Implementation

Several details of the numerical implementation are relevant to successful and accurate use of the body force method, some of which are not explicitly mentioned in the previous literature.

All the integrals in Eqs. (3) to (6) can be carried out in closed form, and are given explicitly in Prime (1994). A word of caution is in order for evaluating the stress in the interval containing the body force, where the stress is singular. Fraga and Hewitt (1983) demonstrated that the principal value of the integral for these functions is obtained by just evaluating the indefinite integral at the endpoints , ignoring the singularity. However, care must be taken in the present case when evaluating the integral. For example , a term of the form *arctan ((x-s)/(y-t))* occurs in evaluating σ_y at the bottom of the slot (Eq. (3)), where $y=t$. Because material is being "removed" above the contour ($y>t$, see Fig. 3), the region of interest is slightly below the contour giving the value of $\arctan(-\infty)$, or $-\pi/2$, rather than $\arctan(\infty)$, or $\pi/2$. The correct value can always be found by offsetting the contour of integration by a small amount towards the material being retained.

The body forces f_{xi} and f_{yi} are taken as constant within each interval. All previous work with the body force method calculated the stresses (right hand side of Eq. (2)) at the center point of each interval. To improve convergence in such work (e.g., Nisitani 1978), results were extrapolated from calculations at say N = 32 and 64 evenly spaced intervals to approximate the value at $N=\infty$ (extrapolated linearly from 1/32 and 1/64 to $1/\infty$). Because in this work the size of the intervals for the free surface body forces will increase as they go to $x = \infty$, as discussed in the next paragraph, this extrapolation based on the number of intervals is less straightforward. Instead, an average stress in each interval replaces the previously used stress at the midpoint. Five point Gauss-Legendre numerical integration (Davis and Rabinowitz 1984) gives the average stress. This was found to converge as accurately as the extrapolation method with no significant increase in computation time.

For the solution to converge, the contour of integration along the free surface ($t=h$, $w<s<s_{max}$) must be substantially longer than the contours for the slot bottom and side. To avoid excessive computation time the intervals along the free surface were allowed to increase in length by a constant fractional amount, $s_{fraction}$. The values of s_{max} and $s_{fraction}$ have a large effect on convergence and error behavior of the solution. Their effects were evaluated by setting E_2 and ν_2 equal to E_1 and ν_1 and comparing to the known solution for a single material (Cheng and Finnie 1993). In comparing the two solutions, the parameters were chosen to be in the typical range found in experimental application of the method to residual stress measurement. Non-dimensionalized by w = 1, they are d = 1, 5, 10, 20 and 30 and x_g = 20, 30 and 40. The value of s_{max} necessary for convergence was found to be approximately independent of cut depth and width and to depend only on the gage distance x_g, varying approximately in the manner shown in Table 1. The effect of varying $s_{fraction}$ was quantified by evaluating the root mean square of the error between this solution and the known solution for the 15 different combinations of d and x_g. The value of s_{max} was held constant at 130, which allowed for reasonable computation times for small values of $s_{fraction}$. Fig. 4 shows the error plotted versus $s_{fraction}$. Since the matrix in Eq. (2) must be inverted once at each cut depth, the calculation time is shown in minutes per cut depth, here for a DECstation 5000/125. From the figure, a value of 0.05 for $s_{fraction}$ was chosen to give a reasonable compromise between error and computation time. This also means that s_{max} can be extended well beyond the minimum value for convergence with little increase in computation time, since the intervals are relatively large for large s.

For the above calculations and the remainder of those in this work, the slot bottom and side combined were divided into 128 intervals of approximately even length. For the case of narrow slots, the minimum number of intervals along the bottom was set at 10. The first interval along the free surface had the same length as the intervals along the slot side. The number of intervals along the free surface was controlled by the choice of s_{max} and $s_{fraction}$ and generally exceeded 128. This degree of discretization gave excellent results.

The discretization of the free surface introduces another source of error. Fig. 5 shows the variation of the compliance within a free surface interval. The particular case shown is for a cut with $w = 1$, $d = 30$, constant slot face loading of $\sigma = 1$, $s_{max} = 200$, and an interval spanning approximately $s = 28.6$ to $s = 30.3$. The solid line is from the known solution, the dashed line is from the layered half-space solution, and the dotted line shows the percentage difference. If the point x_g is at least 5 percent of the interval length away from the end of the interval, the error is ±1 percent or less. In all calculations, the discretization was controlled to ensure that x_g was not too close to an interval endpoint. In applying these calculations to experimental stress measurement, strain at a point is **not** the quantity of interest. Rather, since a strain gage of finite length is used, the average strain over the gage length is important. To calculate this, the discretization of the free surface is adjusted near the gage to place an integer number, n, of evenly spaced intervals within the gage length. Within each interval the average stress is calculated using five point numerical integration, which was confirmed to satisfactorily give the average over a variation like that in Fig. 5. Then the average of the stresses in the n intervals was taken as the compliance for the gage length.

Results and Discussion

Because the number of variables is so large (slot width and depth, layer thickness, location of strain measurement, two elastic constants in each material, variation of loading), it is not possible to present graphical results that would apply for all situations. Rather, results are shown that illustrate the basic trends with respect to the important variables and that illuminate possible errors if simpler solutions, such as ignoring the material properties of the substrate, are used. To facilitate comparison, the compliances are non-dimensionalized. Uniform normal loading on the slot face with a magnitude of 1 is considered. Although compliances for more complex variations in stress are crucial for measuring residual stress, by themselves they provide little additional insight. Compliance is given as stress on the free surface rather than strain, $\sigma_x(x_g)$ rather than $\varepsilon_x(x_g) = \sigma_x(x_g) / E_1'$. This makes the compliance a function of the ratios of the elastic moduli, E_2/E_1, or shear moduli, G_2/G_1, rather than of

their magnitudes. Note that Poisson's ratio is already a non-dimensional quantity and its value for each of the two materials appears independently rather than as a ratio in the solutions. For results looking at the effects of the elastic moduli, both Poisson's ratios are taken as 0.25.

To apply this method to residual stress measurement, the strain gage should be placed where the compliance changes rapidly with an extension in the cut depth. This allows the stress in that region to be determined. Fig. 6 shows the compliance versus cut depth for different values of gage placement. The particular case shown is for $E_2/E_1 = 0.5$ and $h = 30$. When d exceeds x_g, the curves tend to flatten out or "saturate." This indicates that at least one strain gage should be placed at x_g no closer than the maximum depth of cut. This effect depends on E_2/E_1 and is less pronounced when E_2 is greater than E_1. The other main consideration for residual stress measurement is the sensitivity, which is maximized for minimum x_g.

Fig. 7 shows the compliance versus E_2/E_1 for several combinations of d and x_g with h held at 30. As expected the substrate modulus has a strong effect on the compliance, as demonstrated by the slope of the curves. The effect appears stronger for a substrate more compliant than the layer, which is the more common situation. Also, the effect appears strongest for x_g close in magnitude to d. As discussed above, this is the optimum location for strain gage placement. This all serves to indicate that the substrate modulus should not be ignored when measuring residual stress in a layered material.

Fig. 8 demonstrates the effect of the proximity of the substrate on the compliance measured at the surface. Several values of the substrate modulus are considered for a fixed combination of slot depth and gage placement. The compliance is compared to the case of $E_2=E_1$, which corresponds to ignoring the presence of the substrate. For this particular geometry, the error from ignoring the substrate drops to less than 10% when the slot depth is less than half of the layer thickness.

Differences between the Poisson's ratios of the two materials can also have a significant effect on the compliance. The results vary with geometry, gage location, and

modulus ratio. But a general result can be stated that for Poisson's ratios differing by 0.1 or more, the compliances vary by 10% or more from the values for equal Poisson's ratios. The direction of the effect is such that for Poisson's ratio greater in the layer than the substrate, the compliance is increased and vice versa.

Table 2 presents compliance results for one particular case chosen to be somewhat typical and to contain a broad range of values. The case chosen is again non-dimensionalized by $w = 1$. The layer thickness, h, is taken as 10 and the depth of cut, d, penetrates to 20, twice the layer thickness. $E_2\ E_1$ is taken as 0.5 and $\nu_1 = \nu_2 = 0.25$. Three gage positions, x_g = 10,30,50, each with a gage length of 5 centered about x_g are considered. Compliances are given for uniform, linearly varying, and quadratically varying stress fields in both the layer and substrate. For the compliances due to stress in the layer, the non-uniform stresses are taken to vary from 1 at the surface to 0 at the interface. For the compliances due to stresses in the substrate, the non-uniform stresses are taken to vary from 1 at the interface to 0 at the final depth of cut, $d = 20$. The results are from the plane strain solution and are given for $E_1' = 1$. These calculations were made using 256 intervals for the slot sides and bottom ($n_1 + n_2$), the free surface discretization extending to $s_{max} = 450$ and with $s_{fraction} = 0.01$. This degree of discretization, along with the use of a finite gage length, allows the results to be convergent to the extent reported in the table. It should be noted that due to saturation effects discussed earlier, the compliances are not monotonically increasing with depth for the closest gage when the depth is greater than 12.

Several avenues exist for direct extension of this work. For the case of a finite substrate, the body force method can still be used to calculate the compliances. A boundary for the free surface of the substrate would need to be considered along with the boundaries for the slot and free surface of the layer. The body force method could also calculate compliances for the case of orthotropic rather than isotropic elastic materials by using the point force solution for that case (Wu and Chou 1982).

Conclusions

The compliances for a slot in a layered half-space were calculated by extending the body force method to new capabilities. The viability of this approach was demonstrated by comparison to a known solution for a simpler case, allowing confidence in results for the previously unsolved case. This solution provides the capability to apply the compliance method to measure residual stress variation with depth in a layer and substrate.

The resulting compliances were shown to have a strong dependence on the elastic properties of both the layer and substrate. The elastic modulus ratio was the primary factor; although the Poisson's ratios also had a significant effect. Special attention was paid to the effect of ignoring the substrate properties in residual stress measurement. Because of the large number of variables involved, no absolute conclusions were drawn. It could be concluded generally that for differences in elastic modulus of 50 percent or more between the two materials, the properties of the substrate had significant impact on the surface strains for slots penetrating to roughly one-half or more of the layer thickness.

Acknowledgment

Dr. Prime's work while a student at U.C. Berkeley was supported by a National Defense Science and Engineering Graduate Fellowship administered by the AFOSR and by a Berkeley Fellowship. Additional work at Los Alamos National Laboratory was performed under the auspices of the U.S. Department of Energy.

References

Cheng, W., and Finnie, I., 1993, "A Comparison of the Strains Due to Edge Cracks and Cuts of Finite Width With Applications to Residual Stress Measurement," ASME JOURNAL OF ENGINEERING MATERIALS AND TECHNOLOGY, Vol. 115, pp. 220-226.

Cheng, W., Finnie. I., Gremaud, M., and Prime, M. B., 1994, "Measurement of Near Surface Residual Stresses Using Electric Discharge Wire Machining," ASME JOURNAL OF ENGINEERING MATERIALS AND TECHNOLOGY, Vol. 116, pp. 1-7.

Davis, P.J., and Rabinowiz , P.R., 1984, *Methods of Numerical Integration*, 2nd edition, Academic Press, Orlando.

Dundurs, J., and Hetényi, M., 1961, "The Elastic Plane With a Circular Insert, Loaded by a Radial Force," *ASME Journal of Applied Mechanics*, Vol. 28, pp. 103-111.

Fraga, W.E., and Hewitt, R.L., 1983, *Implementation of Nisitani's Body Force Method For the Solution of Notch Problems, Aeronautical Note NAE-AN-17*, National Aeronautical Establishment (Canada).

Frasier, J. T., and Rongved, L., 1957, "Force in the Plane of Two Joined Semi-Infinite Plates," *ASME Journal of Applied Mechanics*, Vol. 24, pp. 582-584.

Hetényi, M., and Dundurs, J., 1962, "The Elastic Plane With a Circular Insert, Loaded by a Tangentially Directed Force," *ASME Journal of Applied Mechanics*, Vol. 29, pp. 362-368.

Nisitani H., 1978, "Solutions of Notch Problems by Body Force Method," *Mechanics of Fracture, Vol 5: Stress Analysis of Notch Problems*, G. C. Sih, ed., pp. 1-68.

Noda, N., Araki, K., and Erdogan, F., 1992, "Stress Intensity Factors in Two Bonded Elastic Layers with a Single Edge Crack Under Various Loading Conditions," *International Journal of Fracture*, Vol. 57, pp. 101-126.

Prime, M.B., 1994, “Residual Stress Measurement in Layered Media,” Ph.D. Thesis, University of California, Berkeley, CA.

Wu, R. S., and Chou, Y. T., 1982, "Line Force in a Two-Phase Orthotropic Medium," *ASME Journal of Applied Mechanics*, Vol. 49, pp. 55-61.

APPENDIX

Point Force Solutions for Two Bonded Half-Spaces

This Appendix contains the point force solution for a point force in two bonded half-spaces, as shown in Fig. 2. The solution given here is that due to Hetényi and Dundurs (1961,1962), changed to the coordinate set of Fig. 2.

Stress in material 1 at *(x,y)* for force in material 1 at *(s,t)*

$$\sigma_{x1}^{P1} = \frac{P(x-s)}{2\pi(\kappa_1+1)}\left[-\frac{\kappa_1+3}{r_1^2}+\frac{4(y-t)^2}{r_1^4}-\frac{3A\kappa_1+B}{r_2^2} -4A\frac{2t^2+(\kappa_1-5)(y+t)t-\kappa_1(y+t)^2}{r_2^4}-32A\frac{(y+t)^2yt}{r_2^6}\right] \tag{A1}$$

$$\sigma_{y1}^{P1} = \frac{P(x-s)}{2\pi(\kappa_1+1)}\left[\frac{\kappa_1-1}{r_1^2}-\frac{4(y-t)^2}{r_1^4}-\frac{A\kappa_1-B}{r_2^2} +4A\frac{2t^2+(\kappa_1-1)(y+t)t-\kappa_1(y+t)^2}{r_2^4}+32A\frac{(y+t)^2yt}{r_2^6}\right] \tag{A2}$$

$$\tau_{xy1}^{P1} = \frac{P}{2\pi(\kappa_1+1)}\left[-\frac{(\kappa_1+3)(y-t)}{r_1^2}+4\frac{(y-t)^3}{r_1^4}+\frac{2A(\kappa_1-1)t-(3A\kappa_1+B)(y+t)}{r_2^2} +4A(y+t)\frac{-6t^2-(\kappa_1-7)(y+t)t+\kappa_1(y+t)^2}{r_2^4}-32A\frac{(y+t)^3yt}{r_2^6}\right] \tag{A3}$$

$$\sigma_{x1}^{Q1} = \frac{Q}{2\pi(\kappa_1+1)}\left[\frac{(\kappa_1-1)(y-t)}{r_1^2}-\frac{4(y-t)(x-s)^2}{r_1^4}+\frac{2A(\kappa_1+3)t-(5A\kappa_1-B)(y+t)}{r_2^2} -4A(y+t)\frac{2t^2+(\kappa_1+1)(y+t)t-\kappa_1(y+t)^2}{r_2^4}-32A\frac{(y+t)(x-s)^2yt}{r_2^6}\right] \tag{A4}$$

$$\sigma_{y1}^{Q1} = \frac{Q}{2\pi(\kappa_1+1)}\left[-\frac{(\kappa_1-1)(y-t)}{r_1^2}-\frac{4(y-t)^3}{r_1^4}+\frac{-2A(\kappa_1-1)t+(A\kappa_1-B)(y+t)}{r_2^2} +4A(y+t)\frac{-6t^2+(\kappa_1+5)(y+t)t-\kappa_1(y+t)^2}{r_2^4}-32A\frac{(y+t)^3yt}{r_2^6}\right] \tag{A5}$$

$$\tau_{xy1}^{Q1} = \frac{Q(x-s)}{2\pi(\kappa_1+1)}\left[-\frac{\kappa_1+3}{r_1^2}+\frac{4(x-s)^2}{r_1^4}-\frac{3A\kappa_1+B}{r_2^2} +4A\frac{6t^2+(\kappa_1-5)(y+t)t+\kappa_1(x-s)^2}{r_2^4}+32A\frac{(x-s)^2yt}{r_2^6}\right] \tag{A6}$$

Stress in material 2 for force in material 1:

$$\sigma_{x2}^{P1} = \frac{P(x-s)}{2\pi(\kappa_1+1)}\left[\frac{-(1-A)\kappa_1-3(1-B)}{r_1^2}-4(y-t)\frac{(B-A)t-(1-B)(y-t)}{r_1^4}\right] \tag{A7}$$

$$\sigma_{y2}^{P1} = \frac{P(x-s)}{2\pi(\kappa_1+1)}\left[\frac{(1-A)\kappa_1-(1-B)}{r_1^2}+4(y-t)\frac{(B-A)t-(1-B)(y-t)}{r_1^4}\right] \tag{A8}$$

$$\tau_{xy2}^{P1} = \frac{P}{2\pi(\kappa_1+1)}\left[\frac{2(B-A)t-((1-A)\kappa_1+3(1-B))(y-t)}{r_1^2} -4(y-t)^2\frac{(B-A)t-(1-B)(y-t)}{r_1^4}\right] \tag{A9}$$

$$\sigma_{x2}^{Q1} = \frac{Q}{2\pi(\kappa_1+1)}\left[\frac{-2(B-A)t+((1-A)\kappa_1-(1-B))(y-t)}{r_1^2} +4(x-s)^2\frac{(B-A)t-(1-B)(y-t)}{r_1^4}\right] \tag{A10}$$

$$\sigma_{y2}^{Q1} = \frac{Q}{2\pi(\kappa_1+1)}\left[\frac{-2(B-A)t-((1-A)\kappa_1-(1-B))(y-t)}{r_1^2} +4(y-t)^2\frac{(B-A)t-(1-B)(y-t)}{r_1^4}\right] \tag{A11}$$

$$\tau_{xy2}^{Q1} = \frac{Q(x-s)}{2\pi(\kappa_1+1)}\left[\frac{-(1-A)\kappa_1-3(1-B)}{r_1^2}+4\frac{(B-A)(y-t)t+(1-B)(x-s)^2}{r_1^4}\right] \tag{A12}$$

where r_1^2 and r_2^2 are defined as follows:

$$r_1^2 = (x-s)^2 + (y-t)^2, r_2^2 = (x-s)^2 + (y+t)^2 \tag{A13}$$

and κ_1, κ_2, A, B, and Γ are defined as follows:

$$\kappa_i = \begin{cases} 3-4\nu_i \text{ (Plane strain i = 1,2)} \\ \dfrac{3-\nu_i}{1+\nu_i} \text{ (Plane stress i = 1,2)} \end{cases} \tag{A14}$$

$$A = \frac{1-\Gamma}{\Gamma\kappa_1 + 1}, \quad B = \frac{\kappa_2 - \Gamma\kappa_1}{\Gamma + \kappa_2}, \quad \Gamma = \frac{G_2}{G_1} \tag{A15}$$

When the point force acts at a point (s,t) in material 2, κ_1, κ_2, and Γ are replaced by κ_2, κ_1, and $1/\Gamma$ respectively in (A1) -(A.12) and (A15). And, of course, 1 and 2 are interchanged in the notation for the stresses (e.g. σ_{x2}^{P1} becomes σ_{x1}^{P2}).

JEMT #96-22 Prime & Finnie

Figure Captions

1. Face loaded slot in layered half-space

2. Point forces in two bonded half-spaces

3. Body forces on integration contour, showing symmetry used for numerical solution

4. Tradeoff between error and computation time as a function of $s_{fraction}$, s_{max} held at 130

5. Error within free surface interval due to discretization

6. Saturation effect. Compliance vs. cut depth for different strain gage locations

7. Effect of substrate modulus. Compliance vs. modulus ratio, different gage locations and slot depths

8. Effect of substrate proximity. Compliance compared to E_2=E_1, as a function of layer thickness

Table Captions

1. Convergence behavior

2. Compliances values for $h = 10$, $w = 1$, $E_2/E_1 = 0.5$, $\nu_1 = \nu_2 = 0.25$

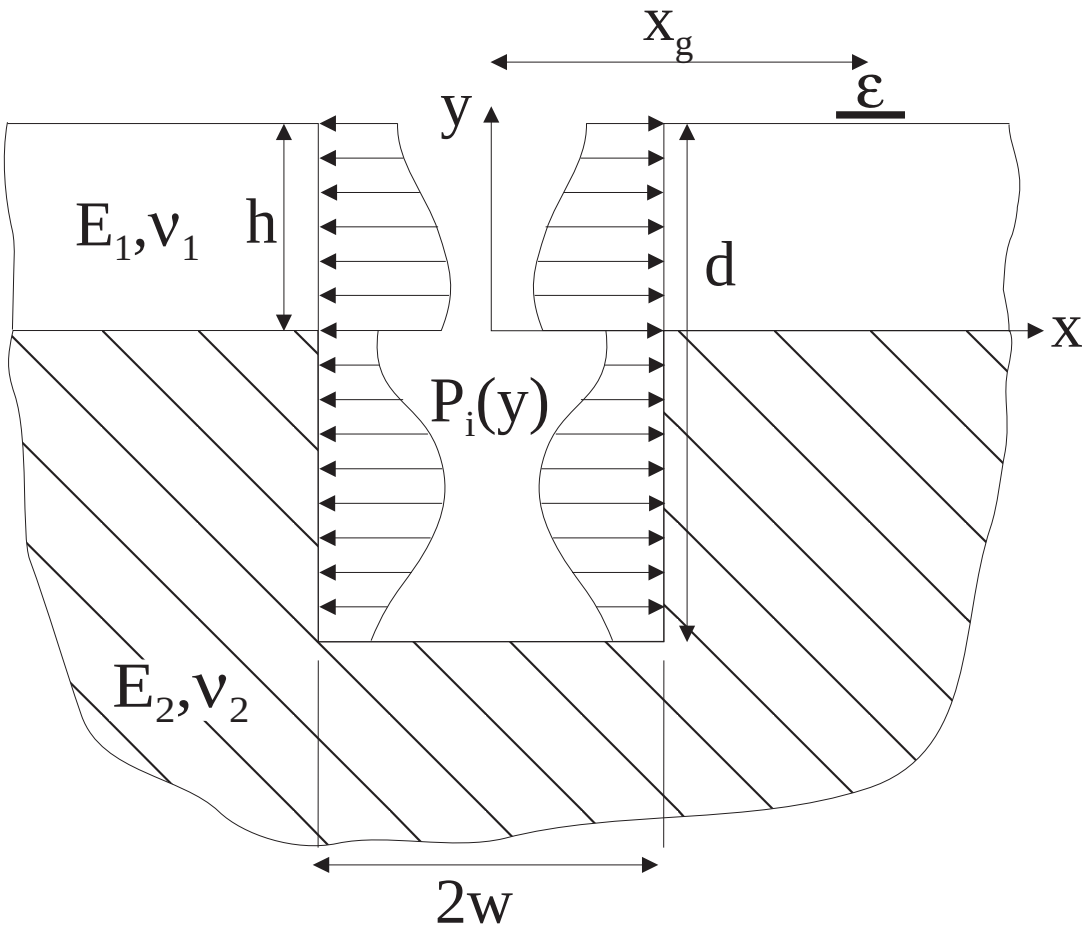

Prime & Finnie Figure 1

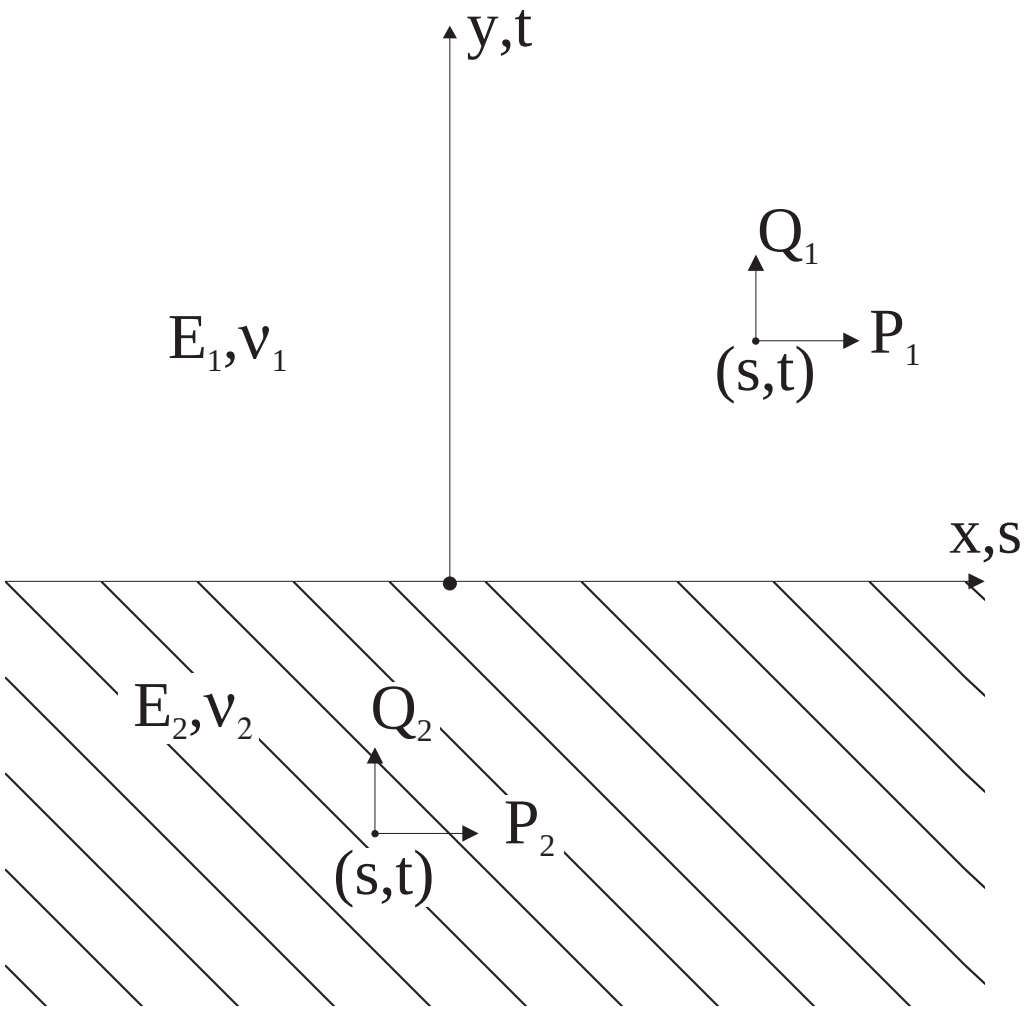

Prime & Finnie Figure 2

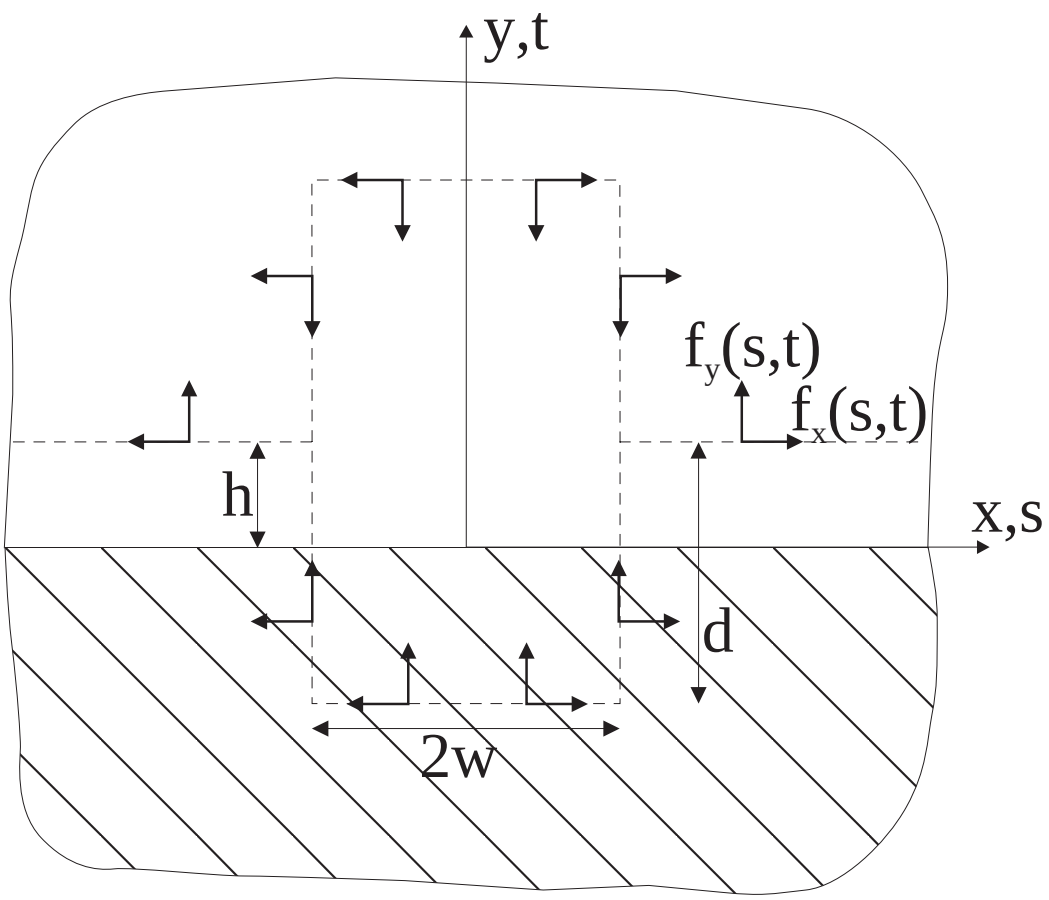

Prime & Finnie Figure 3

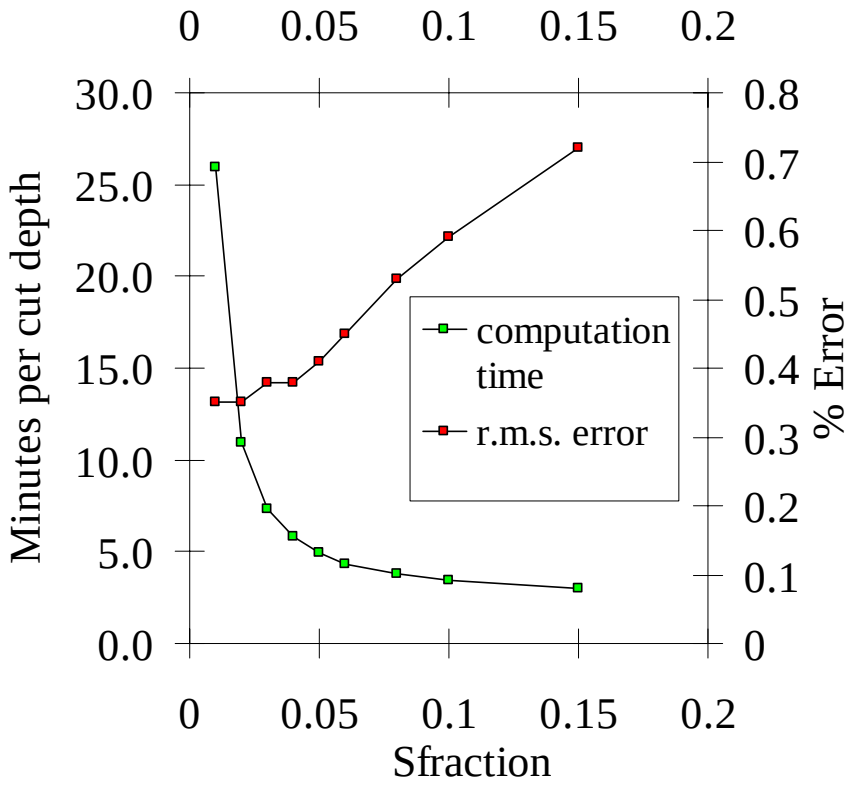

Figure 4.

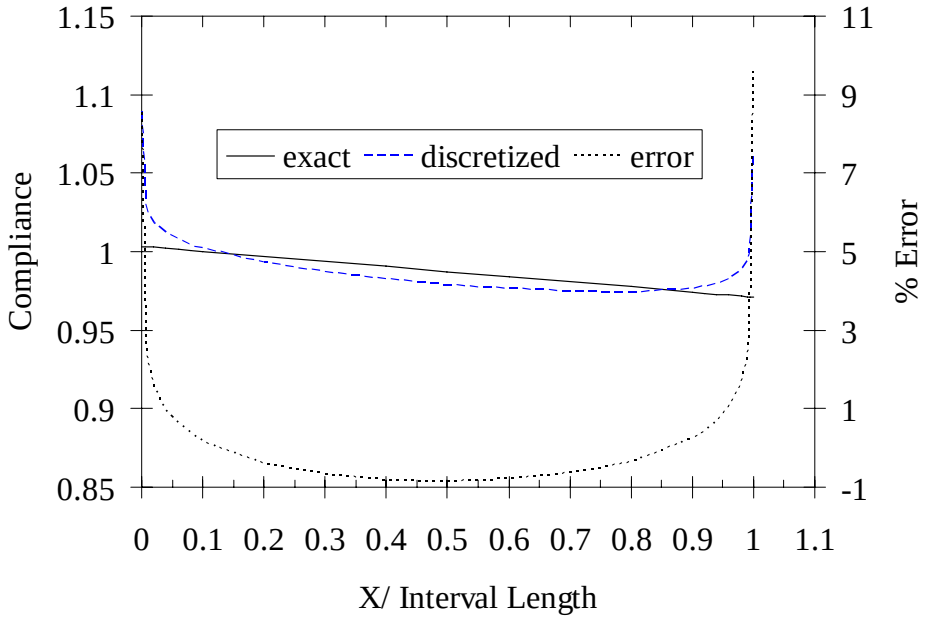

Figure 5.

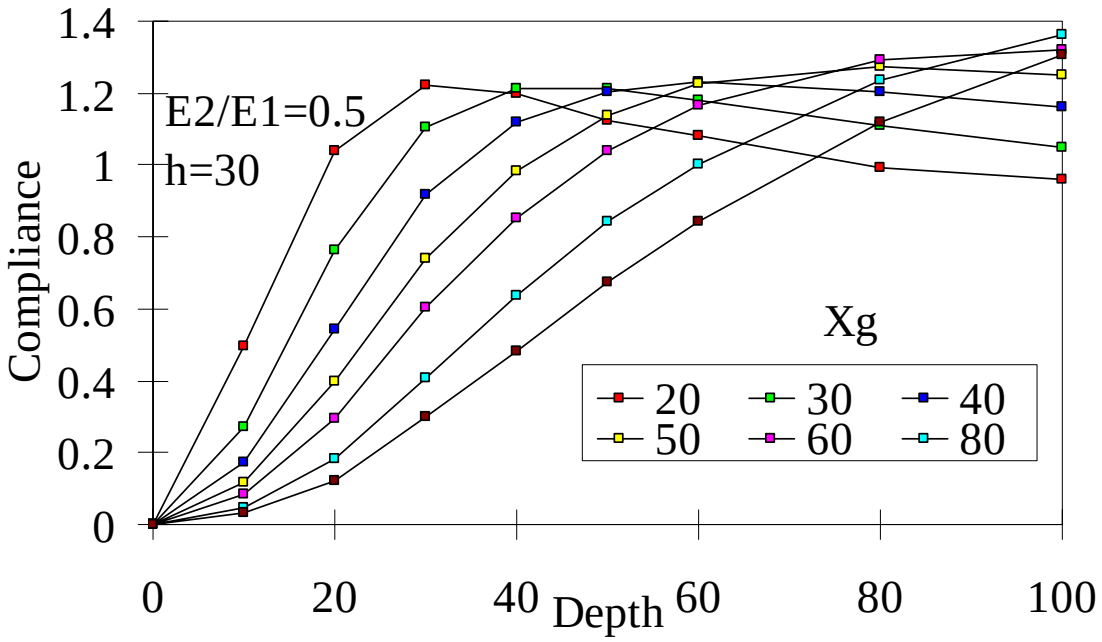

Figure 6.

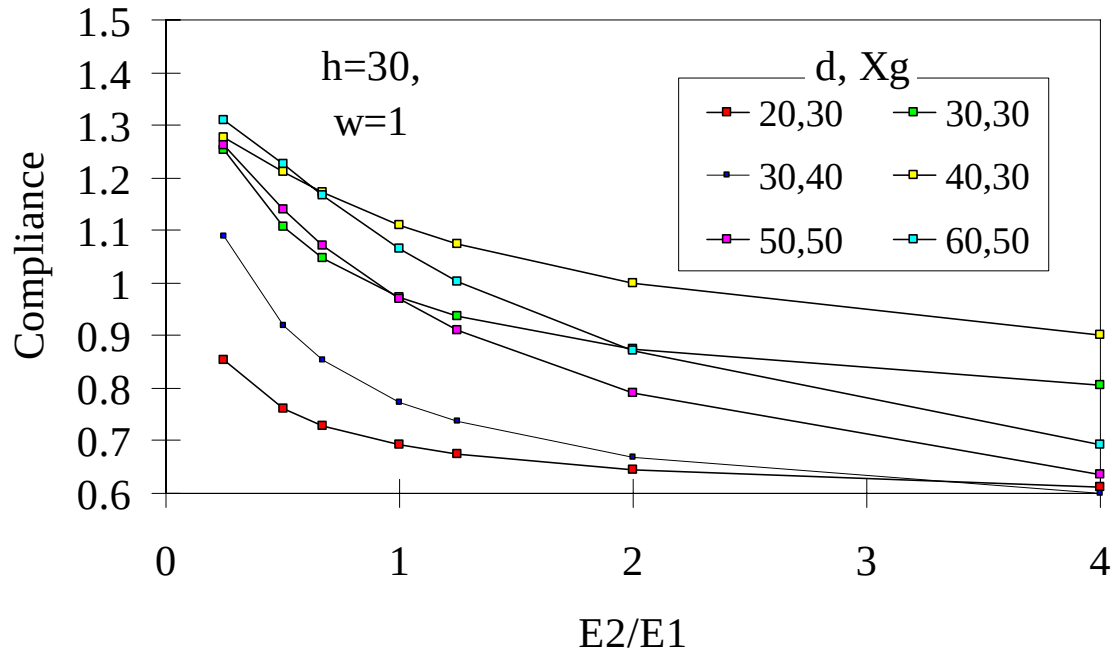

Figure 7.

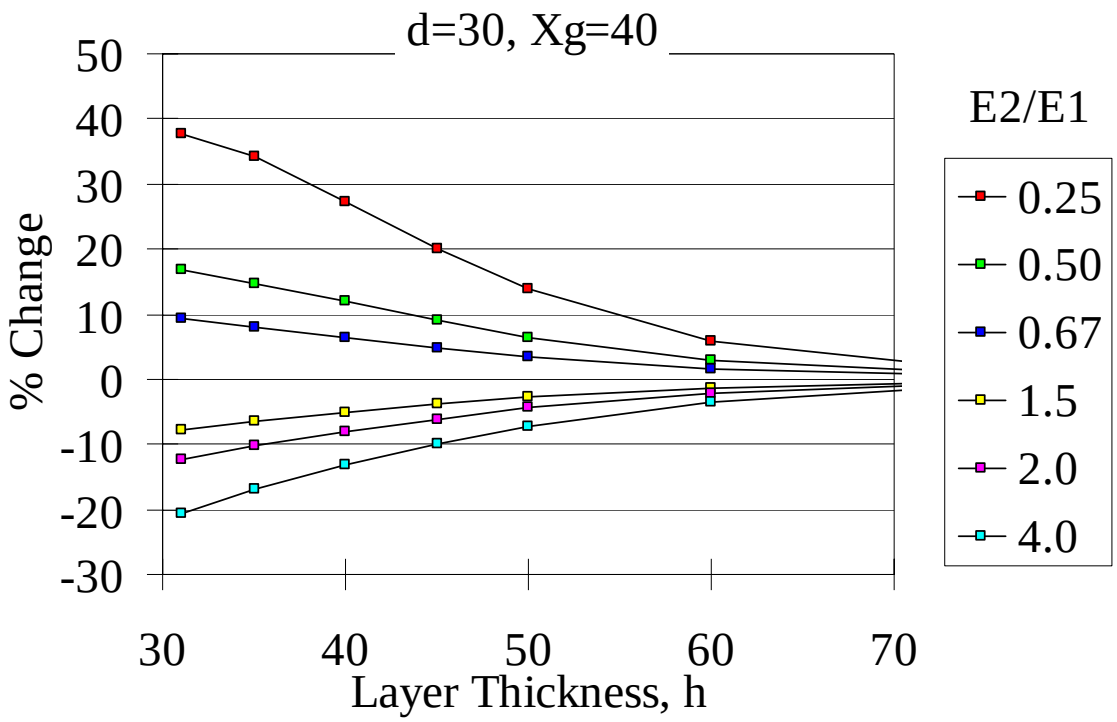
d=30, Xg=40
% Change
50
40
30
20
10
0
-10
-20
-30
30
40
50
60
70
Layer Thickness, h
E2/E1
0.25
0.50
0.67
1.5
2.0
4.0

Figure 8.

Gage distance, x_g	s_{max} for convergence
20	120
30	200
40	300

Table 1. Convergence behavior

Gage	Stress In Layer			Stress In Substrate		
Distance	uniform	linear	quadratic	uniform	linear	quadratic
			depth = 2			
10	0.1449	0.1325	0.1216	–	–	–
30	0.01682	0.01534	0.01404	–	–	–
50	0.00634	0.00578	0.00528	–	–	–
			depth = 4			
10	0.4298	0.3619	0.3096	–	–	–
30	0.0593	0.04921	0.04155	–	–	–
50	0.02310	0.01913	0.01612	–	–	–
			depth=8			
10	0.9675	0.7102	0.5571	–	–	–
30	0.2197	0.1481	0.1099	–	–	–
50	0.09414	0.0626	0.04601	–	–	–
			depth = 12			
10	1.1704	0.8108	0.6236	0.0079	0.0075	0.0071
30	0.4456	0.2519	0.1772	0.0364	0.0333	0.0306
50	0.2095	0.1153	0.0801	0.0199	0.0182	0.0167
			depth = 16			
10	1.188	0.820	0.630	0.0050	0.0074	0.0083
30	0.5661	0.3109	0.2163	0.1500	0.1143	0.0910
50	0.2804	0.1498	0.1030	0.0896	0.0675	0.0532
			depth = 20			
10	1.179	0.816	0.627	-0.0199	-0.0021	0.0031
30	0.6471	0.3511	0.2430	0.2755	0.1725	0.1263
50	0.3382	0.1785	0.1220	0.1831	0.1098	0.0787

Table 2. Compliances values for $h = 10$, $w = 1$, $E_2/E_1 = 0.5$, $\nu_1 = \nu_2 = 0.25$